Proceedings of the 3rd International Symposium on Shape Casting held at the 2009 TMS Annual Meeting, 15-19 February 2009, San Francisco, California, USA, pp. 71-78

OXIDE ENTRAINMENT STRUCTURES IN HORIZONTAL RUNNING SYSTEMS

C Reilly[1], N.R Green[2] and M.R. Jolly[1]

[1]School of Mechanical Engineering, University of Birmingham, UK
[2]School of Metallurgy and Materials, University of Birmingham, UK

Keywords: Casting, Oxide, Quality Assessment, Entrainment, Running System

Abstract

During the transient phase of filling a casting running system surface turbulence can cause the entrainment of oxide films into the bulk liquid. Research has shown that these are detrimental to the material's integrity. Common mechanisms for this entrainment include returning waves, arising during filling of the runner bar, and plunging jets, found when pouring into a basin. One of these, the returning wave, has been studied in greater depth, using real-time X-ray and process modelling techniques alongside the application of physical principals. It has been concluded that when developed, returning waves cannot attain the more stable and less entraining tranquil flow regime desirable in the running system of castings.

Introduction

Real time X-ray studies have shown that when a stream of fluid impacts the end of a runner bar a chaotic flow regime is produced for a short period in this locality. This chaotic regime develops into a returning wave. These waves are known to be highly entraining and detrimental to casting integrity as they entrain double oxide films [1, 2]. Such flow phenomena have previously been observed to resemble hydraulic jumps.

It was the original intention of this research to determine the threshold flow conditions that lead to formation of, and gas entrainment by, hydraulic jumps in liquid metals. A threshold has been shown experimentally in water, where the hydraulic jump is relatively well understood and the theory for which is reliant on certain assumptions being made [3]. One of these; the assumption that surface tension effects are negligible may not hold true however for most liquid metals. After detailed experimental investigations, contrary to what had been shown through simulation previously [4], it was not possible to create hydraulic jumps within an open channel running system at liquid metal velocities in excess of 3 ms^{-1}, flow depths of 0.01 m and flow distances of 1 m. Thus it was concluded a 'trigger' is required to initiate a 'hydraulic jump' type structure. It was observed that in this geometrical configuration only the return wave generated at the end of the runner created such a structure.

Returning waves have been known as entraining hydraulic structures but little work has been undertaken thus far on characterising them. This work has concentrated on attempting to understand the trigger, using a combination of experimental, numerical and first principles methods, in order to allow further insight into the constrained return wave found in running systems.

The foundry engineer can calculate the returning wave velocity for a constrained wave in a runner bar of uniform thickness via the principles of conservation of volume [3], as represented in equation 1. The difficulty comes in predicting the height of the returning wave (and thus its velocity) when the constraint is removed.

Past work has shown how casting integrity is greatest when the system fills in a tranquil manner. However, if return waves are formed the persistence of these is critical in determining their overall damage to casting integrity [5, 6]. Although the use of low profile runners, *i.e*. a height of less than the sessile drop height of the fluid has been advocated to stop such waves forming [7] this is not always possible; for example due to manufacturing constraints or lack of flow control for multiple gated systems.

Criterion Development

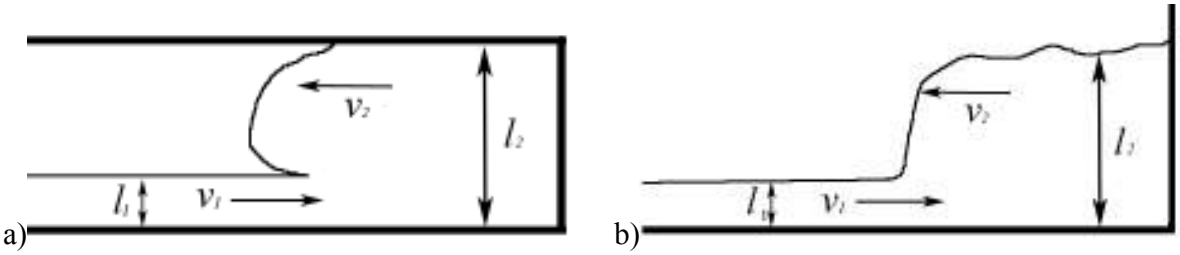

Figure.1 a) Constrained flow schematic b)Unconstrained flow schematic

Constrained Flow

For a constrained return wave the velocity can be calculated from principles of conservation of volume [3] as shown in Equation 1 where v_1 is the inflowing fluid velocity (ms^{-1}), l_1 is the inflowing fluid height (m), and l_2 is the runner bar height (m). This is shown in Figure 1(a).

$$v_2 = \frac{l_1 . v_1}{l_2 - l_1} \tag{1}$$

However, this condition, is only true for the section of the running system between the end of the runner and the in-gate (Section A, Figure 2) To calculate the return wave velocity for the area between the in-gate and downsprue (Section B, Figure 2) it is necessary to account for the fluid volume which is flowing into the casting volume.
For most industrial castings this is extremely difficult to determine from first principles without making assumptions that severely limit the accuracy of the calculation. One difficulty comes from the fact that the volume flowing into the casting varies with time.

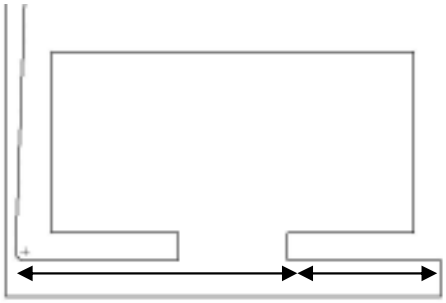

Figure 2. Casting schematic

Unconstrained Flow

For an unconstrained returning wave the velocity for a channel of uniform and unit thickness can be calculated by balancing the energy equation, as shown in the derivation below: (Figure 1b)

Incoming flow kinetic energy	+	Potential energy of fluid height l_1	=	Returning wave kinetic energy	+	Potential energy of fluid height l_2

The potential energy (PE) of the of incoming flow per unit width per unit time = *mgh* where *m* is the mass, *g* the acceleration due to gravity and *h* is a length

$$m = \rho l_1 v_1 \quad \text{and} \quad h = \frac{l_1}{2}, \text{ therefore PE} = \frac{1}{2}\rho l_1^2 v_1 g \tag{2}$$

where ρ is the fluid density (kgm^{-3}). The kinetic energy (KE) of the incoming flow per unit width per unit time = $\frac{1}{2}mv_1^2$

$$\text{As } m = \rho v_1 l_1 \text{ from (2) then KE} = \frac{1}{2}\rho l_1 v_1^3 \tag{3}$$

Potential energy of return wave per unit width per unit time = *mgh*

$$m = \rho(l_2 - l_1)v_2 \quad \text{and} \quad h = \left(\frac{l_2 - l_1}{2} + l_1\right) \text{ therefore PE} = \frac{1}{2}\rho(l_2 - l_1)v_2\left(\frac{l_2 - l_1}{2} + l_1\right)g \tag{4}$$

Kinetic energy of return wave per unit width per unit time $= \frac{1}{2}mv_2^2$; where wave depth $= l_2 - l_1$,

$$m = \rho(l_2 - l_1)v_2, \text{ therefore KE} = \frac{1}{2}\rho(l_2 - l_1)v_2^3 \tag{5}$$

Balancing the energies of incoming and returning flows (energy flux) gives;

$$\frac{1}{2}\rho g l_1^2 v_1 + \frac{1}{2}\rho l_1 v_1^3 = \frac{1}{2}\rho(l_2 - l_1)v_2\left(\frac{l_2 - l_1}{2} + l_1\right)g + \frac{1}{2}\rho(l_2 - l_1)v_2^3 \tag{6}$$

$$g l_1^2 v_1 + l_1 v_1^3 = 2(l_2 - l_1)v_2\left(\frac{l_2 - l_1}{2} + l_1\right)g + (l_2 - l_1)v_2^3 \tag{7}$$

For this equation to be of use it needs to be solved independently of $v_2$or l_2. Substituting v_2 from equation 1 and simplifying gives;

$$g l_1^2 v_1 + l_1 v_1^3 = l_1.v_1\left((l_2 - l_1) + 2l_1\right)g + (l_2 - l_1)\left(\frac{l_1.v_1}{l_2 - l_1}\right)^3 \tag{8}$$

Rearranging;

$$0 = \left(g l_1^2 v_1 + l_1 v_1^3\right) - \left(l_1.v_1\left((l_2 - l_1) + 2l_1\right)g + (l_2 - l_1)\left(\frac{l_1.v_1}{l_2 - l_1}\right)^3\right) \tag{9}$$

Equation 10 was solved in Matlab using the 'solve' function. The solutions are 0 and equation10;

$$l_2 = \frac{1}{2g}\left(v_1^2 + 2gl_1 \pm \sqrt{-4gl_1 v_1^2 + v_1^4}\right) \tag{10}$$

Upon determining l_2 the velocity, v_2 of an unconstrained wave can be calculated by substitution into equation 1 giving the results plotted in Figures 3 through 6.

Experimental Design

Moulds were cast in a real-time X-ray flow imaging facility, the principles of which have been reported previously [8]. Castings (Figure 3) were poured in resin bonded silica sand moulds (AFS grade 60 sand) using aluminium alloy 2L99. A range of sprue heights whose design conforms to that defined by Campbell [1] were used to adjust the metal flow velocity and mass flow rate. The cast weight was 11 kg, the pouring temperature 760 ºC and the pouring was controlled using a robotic system. Filling was viewed using real-time X-ray radiography to allow the qualitative assessment of the transient flow. Flow images were captured at a rate of 100 s^{-1} and resolution 800×600 pixels over a field of view of approximately 200×150 mm.

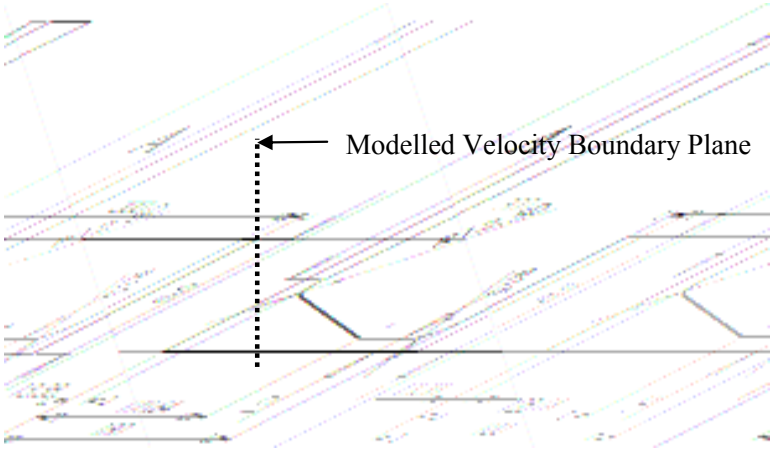

Trial	A (mm)
1	70
2	105
3	120
4	200
5	360

Figure 3. Experimental mould (all dimensions in mm)

Process Modelling

Flow-3D [9], (a commercially available CFD code) was used to model the casting experiments. A velocity boundary condition was imposed on the plane shown in Figure 3. Velocities of 1.02, 1.1, 1.18, 1.25 and 1.37 ms^{-1} measured from the experimental results for v_1 from Trials 1 through 5 respectively were used as the boundary condition. Only the section of the mould to the right of the velocity boundary plane shown in Figure 3 was modelled. This allowed a more accurate comparison with the theoretical results as v_1 could be kept constant. However, it should be noted that with this approach the simulations may not fully match the real time X-ray results as during the transient filling phase when the downsprue is backfilling the pressure (and therefore velocity) of the fluid flowing through this section would not be expected to have reached the stable equilibrium as modelled.

Results

The results shown in Table 1 and Figures 4 and 5 show how, for a given set of inlet parameters there are two alternative flow regimes; rapid and tranquil flow. The exception for this is where the energy is at a minimum at the 'nose' of the returning wave depth curve. This is analogous to the energy nose observed in hydraulic jump structures [3].

Rapid flow is when the flow takes the high velocity and low wave height parameter. This regime is normally considered much more turbulent and highly entraining than the tranquil regime were the fluid takes the alternative parameters, namely a deep but slow moving flow. A much reduced, if at all, entraining regime.

Figures 6 to 8 show examples of the experimental results. These show how initially the returning wave (circled in Figure 7) takes the rapid flow form before immediately jumping to try and attain the tranquil regime.

Experimental results also show the returning wave periodically retreating along the runner bar, giving an insight of the potential magnitude of turbulent energy losses caused by the shearing in the region of the wave front. Figure 6b, 0.2-0.4 s shows clearly that the wave has progressed very little in 0.2 seconds when compared with the distance travelled between 0.4 and 0.6 s.

Figure 7 shows two different but clearly defined examples of the initial wave of low height followed by a jump. This initial wave size matches the theoretical values calculated for Trials 1 through 5, where l_1 equals 10 mm ±2 mm and v_1 ranges from 1.02 ms^{-1} to 1.35 ms^{-1}. This gives l_2 a range of values between 20.6 to 21.2 mm; equation 10. This is obviously beyond the accuracy available with the real-time X-ray equipment of ±2 mm at a turbulent free surface. However, this flow form can be seen in all experimental trails, with the theoretical height of the initial wave lying within the experimental accuracy of the equipment. The modelled results gave l_2 values of 20-22 mm frequently throughout all modelled trials. However, with such waves being unstable the accurate definition of this can be troublesome for many cases. For example Figure 6 b) 0.6 s where the nose of the wave can be seen to be of uniform angle with l_2 values rising from 15 to 35 mm with no clear definition of the 21mm initial wave.

It can be seen in Figure 8 that even with an unconstrained wave there is entrainment of oxide films and bubbles present at the wave front, even for this relatively low energy condition. Further work is required to define if an entrainment threshold exists for a stable wave or whether the rapid regime is entraining for all inlet conditions.

The modelled flow results showed good agreement with the experimental and first principles models with respect to the flow profiles observed. Figure 9 shows example images of the returning wave form that initially advances in the rapid form before immediately attempting to jump to the tranquil form.

Figures 10 and 11 summarise experimental and *Flow 3D* results which correlate favourably. In reviewing these it must be remembered that;

i) There are large errors associated with extracting data from both the experimental results and modelled results. The error within the results is significant due to the following factors;

- The wave has not reached equilibrium, meaning results vary heavily depending on the time frame(s) chosen for analysis. Future work should look at using longer channels to allow a stable wave to form, giving more accurate analysis.
- The bulking effect of air being entrained into the liquid changes the local fluid density; this effect it not considered in either the theoretical calculations or the model.
- The measuring of the incoming fluid velocity v_1 is not accurate as the initial jet is unrepresentative of the steady state condition and the effective head height is constantly varying as the sprue and basin back fill during this initial transient period.
- Difficulties in assessing experimental fluid depth; accuracy being ±2 mm.
- Parallax error from the camera.

ii) The wave height plotted in these figures is not a measure of the initial rapid wave height, but the height the wave attains when trying to reach the tranquil flow regime.

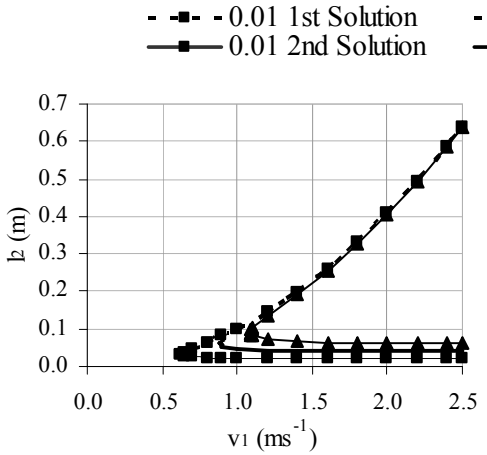

Figure 4. v_1 Vs l_2 (l_1 of 0.01, 0.02 and 0.03 m)

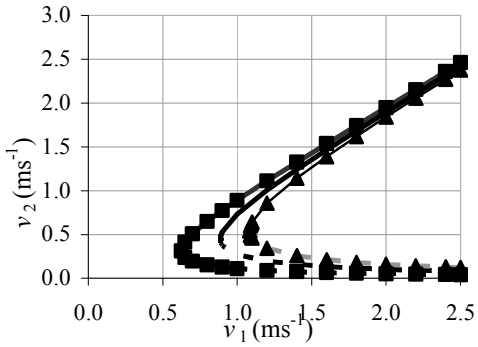

Figure 5. v_1 Vs v_2 (l_1 of 0.01, 0.02 and 0.03 m)

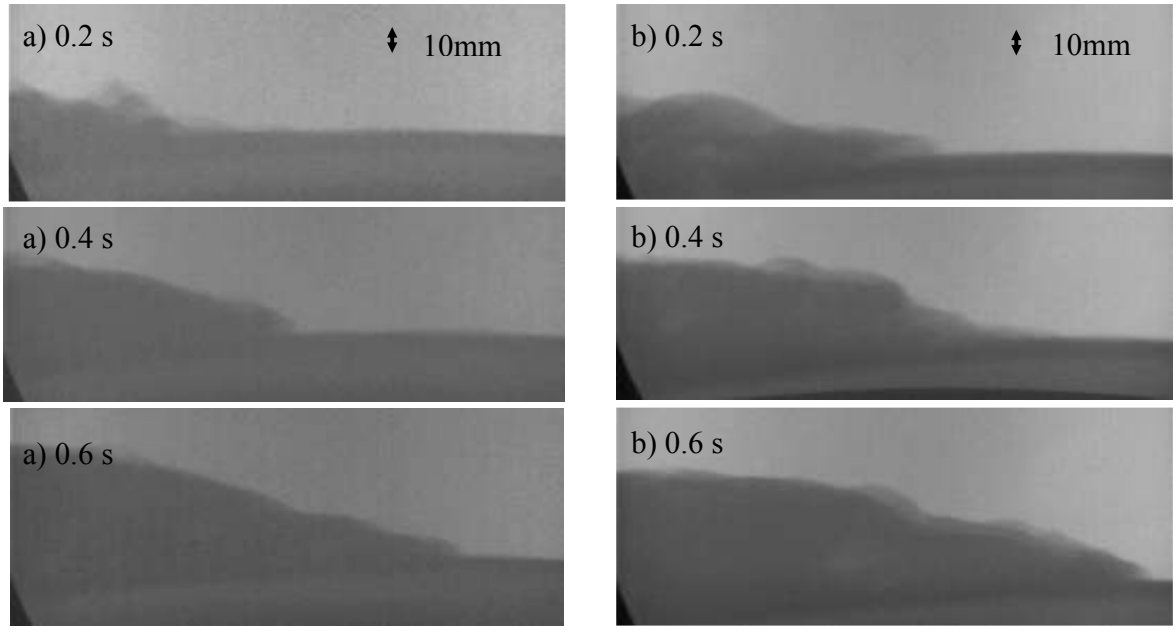

Figure 6. Real –time X-ray of returning waves in a)Trials1 and b) Trial 2

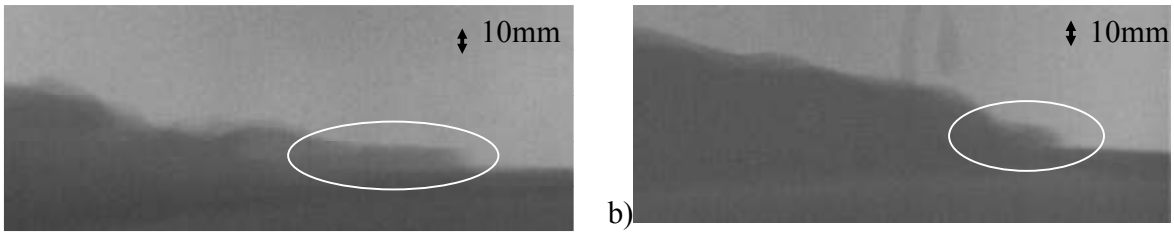

Figure 7. Images of initial wave height followed by a hydraulic jump. Ringed areas denote regions where the initial wave heights were measured.

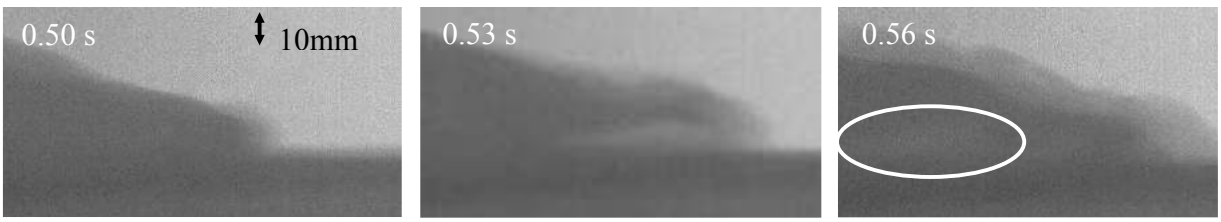

Figure 8. Instability in advancing flow front leading to entrainment of an air bubble; Trial 2

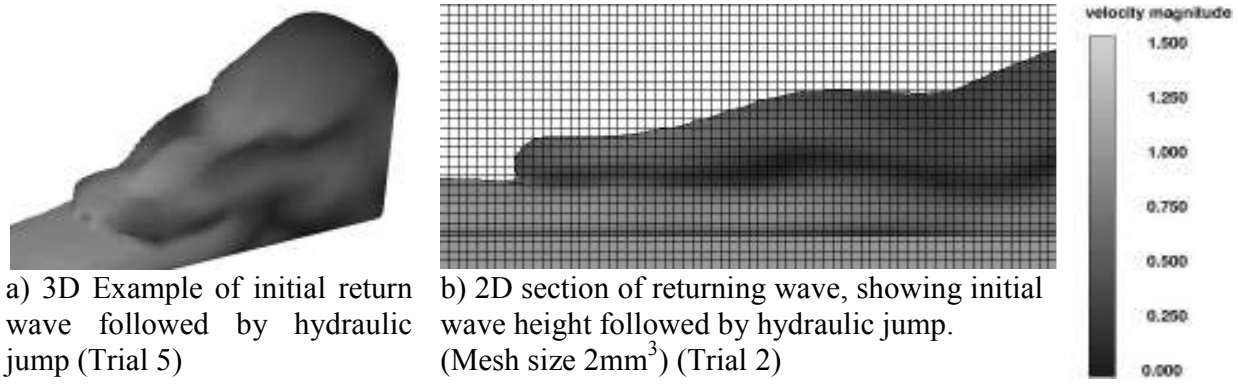

a) 3D Example of initial return wave followed by hydraulic jump (Trial 5)

b) 2D section of returning wave, showing initial wave height followed by hydraulic jump. (Mesh size 2mm^3) (Trial 2)

Figure 9. Examples of modelled two stage returning waves.

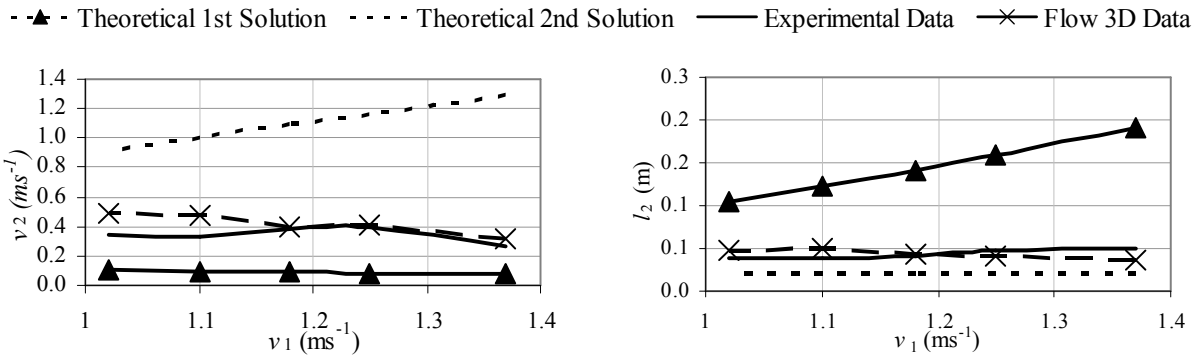

Figure 10. Plot of theoretical, modelled and measured return wave velocities.

Figure 11. Plot of theoretical, modelled and measured return wave heights.

Discussion

It should be noted that the velocity v_2 and height l_2 of the returning wave for both constrained and unconstrained waves, are dependent on both the approach velocity v_1 and fluid depth l_1, but independent of the physical characteristics of the fluid, for example density, surface tension and viscosity (Equation 8). In this study the well structured incoming flow had a Froude number in the range 3.3 to 4.4. In many casting systems even higher values could reasonably be expected. As stated in the introduction, the flow of liquid aluminium alloys under such inlet conditions has not been observed to initiate a hydraulic jump in a continuous open channel flow. The reflected wave and the shearing interface are essential components of the flow to initiate entrainment.

The presence of two stable flow depths suggested by the simple energy balance is analogous to that derived for an hydraulic jump [3]. In this series of experiments the greater (tranquil) calculated flow depth has not been observed and the predicted height remains somewhat surprising. It also appears to be the case that the thin jet forms ahead of the main returning flow and thus such systems will always be prone to severe entrainment. Therefore reduction of the persistence of the entrainment event is key to achieving optimum casting integrity [6]. One approach applied successfully in industry is the application of reticulated foam filters.

The observed returning flow depths suggest significant energy loss, due principally to shearing at the wave front, bulk turbulence and the bulking affect of air entrainment. It should also be noted that the tranquil depth of flow is far greater than that which could be accommodated in the runner bar of a casting design within normal parameters. Therefore the flow becomes

constrained, causing the return wave to increase its velocity along the runner bar with high levels of entrainment but low persistence. The turbulent energy loss can be quantified by calculating the energy difference between the flow obtained experimentally and that associated with either the rapid or tranquil flow regime using Equation 7. Calculation based upon the average return wave velocity and height derived from experimental data shows energy losses in the system of between 50 and 73%. This is clearly well described within the RNG turbulence model.

The above findings show that there is no way to fill a casting runner bar without the entrainment of oxide films if the system is not a single pass design [1]. Single pass systems have been shown to be beneficial to casting integrity but are not appropriate for systems with multiple gates or where large flow rates have to be used because of the casting geometry aspect ratios. Where single pass designs are not possible it appears that running system geometry should concentrate on dissipation of the return wave energy. Further research is required in this area.

Conclusions

1. Within the geometries studied it is impossible for the tranquil state to be achieved without an hydraulic jump and its inherent energy dissipation.
2. The trigger for an hydraulic jump to occur within a casting runner is the back wave.
3. Returning back waves always develop an initial rapid regime before immediately trying to obtain stable tranquil state through an hydraulic jump.
4. Minimisation of the persistence of free surface entrainment is crucial to give maximum casting integrity.
5. Correlation between the theoretical model proposed for an unconstrained wave and experimental data is good. Further data are required for definitive validation

Acknowledgments

The authors would like to acknowledge the help of The School of Mechanical Engineering, The University of Birmingham for sponsoring the PhD of CR, the support of Flow Science Inc and the EPSRC support of NG's chair (EP/D505569/1).

References

1. J. Campbell, *Castings 2nd Edition* (Butterworth Heinemann, 2003) 71.
2. N.R Green and J. Campbell, "Influence in Oxide Film Filling Defects on the Strength of Al-7si-Mg Alloy Castings", *Transactions of the American foundry society,* 114 (1994) 341 -347.
3. B. S. Massey, *Mechanics of Fluids 6th Edition* (Chapman & Hall, 1992).365-369.
4. F.-Y. Hsu, "Further Developments of Running Systems for Aluminium Castings", (PhD Thesis, The University of Birmingham, 2003) 137-138.
5. C. Reilly, "Surge Control Systems for Gravity Castings", (Final Year Project, The University of Birmingham, 2006) 45-72.
6. C. Reilly, N. R. Green, M. R. Jolly and J. C. Gebelin, "Using the Calculated Fr Number for Quality Assessment of Casting Filling Methods", *Modelling of casting, welding and advanced solidification process XII*. (2009).
7. J. Campbell, *Castings Practice: The 10 Rules of Casting* (Butterworth Heinemann, 2004) 41-47
8. M. Cox, R. A. Harding and J. Campbell, "Optimised Running System Design for Bottom Filled Aluminium Alloy 2l99 Investment Castings", *Materials science and technology* 19 (2003) 613-625
9. *Flow3D*, www.flow3d.com.